Automated Detection of Road Manhole and Sewer Well Covers From Mobile LiDAR Point Clouds

Article *in* IEEE Geoscience and Remote Sensing Letters · September 2014

DOI: 10.1109/LGRS.2014.2301195

CITATIONS
15

READS
173

5 authors, including:

Yongtao Yu
Huaiyin Institute of Technology
41 PUBLICATIONS **370** CITATIONS
SEE PROFILE

Jonathan Li
University of Waterloo
254 PUBLICATIONS **3,243** CITATIONS
SEE PROFILE

Haiyan Guan
Nanjing University of Information Science & …
52 PUBLICATIONS **428** CITATIONS
SEE PROFILE

Cheng Wang
Xiamen University
157 PUBLICATIONS **894** CITATIONS
SEE PROFILE

Automated Detection of Road Manhole and Sewer Well Covers From Mobile LiDAR Point Clouds

Yongtao Yu, Jonathan Li, *Senior Member, IEEE*, Haiyan Guan, Cheng Wang, *Member, IEEE*, and Jun Yu

***Abstract*—A novel object detection algorithm is developed for automatically detecting road manhole and sewer well covers from mobile light detection and ranging point clouds. This algorithm takes advantage of a marked point process of disks and rectangles to model the locations of manhole and sewer well covers and their geometric dimensions. A reversible jump Markov chain Monte Carlo algorithm is implemented for simulating the posterior distribution obtained using a Bayesian paradigm. The detection results obtained from the road surface point clouds acquired by a RIEGL VMX-450 system show that the manhole and sewer well covers can be detected automatically and accurately. The performance achieved using the proposed algorithm is much more accurate and effective than those of the other three existing algorithms.**

***Index Terms*—Manhole, marked point process, mobile light detection and ranging (LiDAR), point cloud, reversible jump Markov chain Monte Carlo (RJMCMC), sewer well.**

I. Introduction

MANHOLES and sewer wells in urban areas are used to conduct rainwater, drainage, power cables, telecommunication cables, and other things. They are usually covered with a metal-made cover to keep things from dropping into the wells. However, if the cover is removed by someone or broken caused by some uncertain factors, it is dangerous to the moving cars and pedestrians. Therefore, efficient and cost-effective means and methods that can monitor potential disasters on the road are urgently in demand. Detecting and monitoring manhole and sewer well covers is greatly important to the transportation infrastructure management department; and it provides a promising and essential way to prevent potential disasters on the road.

Existing methods to the detection of manhole and sewer well covers are based on the digital imagery. Tanaka and Mouri [1] proposed to detect manhole covers from road surface images based on morphological techniques. First, a black top-hat operation with disk-shaped structure elements was used to extract round-shaped components. Then, a masking operation was applied to the round-shaped components with a thresholded input image. Finally, manhole covers were obtained by simply eliminating the regions with small areas. Instead of analyzing the intensity difference of road surface imagery between the object of interest and its surroundings, the separability and uniformity of the image intensity distributions were studied in [2] to detect circular objects using the Bhattacharyya coefficient. Three indicators, including circular object indicator, oriented separability indicator, and uniformity indicator, were defined and used to achieve robust detection. Challenges resulting from frequent occlusions, regular changes in illumination conditions, and substantial viewpoint variances bring big problems to the detection, recognition, and 3-D localization of manhole covers from the images captured by moving vans. As a result, a multi-view method was presented in [3] to detect manhole covers by combining 2-D and 3-D techniques. Considering the complex background of road surface images, an improved classical Hough transform was proposed in [4] to detect manhole covers.

In the past decades, light detection and ranging (LiDAR) technology has been rapidly developed and used by a variety of applications [5], [6]. The point cloud data acquired by the LiDAR systems have been used for the detection and extraction of various objects, such as trees [7]–[9], roads [10], and buildings [11]–[13]. Mobile LiDAR systems are state-of-the-art laser scanning products in the current market. Due to the long-range, high-speed, and low-cost data acquisition, mobile LiDAR systems have been widely used in the fields of surveying and mapping. Basically, mobile LiDAR systems use near-infrared radiations to measure the topology of an object and collect the reflectance returned by the measured objects. Due to the high pulse repetition rate (e.g., 550 kHz), the density of the acquired point clouds is very high (e.g., approximately 4000 points/m^2 on the road surface). Therefore, mobile LiDAR systems provide a suitable solution to detecting manhole and sewer well covers on road surfaces.

In this letter, we present an automated algorithm to detect manhole and sewer well covers from mobile LiDAR point clouds based on a marked point process of disks and rectangles. Different from the existing object detection methods based on the marked point process, our stochastic object-oriented algorithm is based on the Bayesian paradigm, which can efficiently process very large volumes of 3-D point clouds covering road surfaces with an unknown number and sizes of manhole and sewer well covers, and adjust the boundaries of all detected targets with low time complexity. The idea behind the marked point process is to model the number and locations of manhole and sewer well covers as point processes and to define their geometries as marks. The road surface point clouds are first rasterized into a georeferenced intensity image based on the

Manuscript received November 5, 2013; revised January 2, 2014; accepted January 15, 2014. This work was supported in part by a Natural Sciences and Engineering Research Council of Canada Discovery Grant and in part by the National Natural Science Foundation of China under Project 61371144.

Y. Yu, C. Wang, and J. Yu are with the School of Information Science and Engineering, Xiamen University, Xiamen, FJ 361005, China.

J. Li is with the Key Laboratory of Underwater Acoustic Communication and Marine Information Technology (Ministry of Education), School of Information Science and Engineering, Xiamen University, Xiamen, FJ 361005, China and also with the GeoSpatial Technology and Remote Sensing Laboratory, Faculty of Environment, University of Waterloo, Waterloo, ON, N2L 3G1, Canada (e-mail: junli@xmu.edu.cn).

H. Guan is with the GeoSpatial Technology and Remote Sensing Laboratory, Faculty of Environment, University of Waterloo, Waterloo, ON, N2L 3G1, Canada.

Color versions of one or more of the figures in this paper are available online at http://ieeexplore.ieee.org.

Digital Object Identifier 10.1109/LGRS.2014.2301195

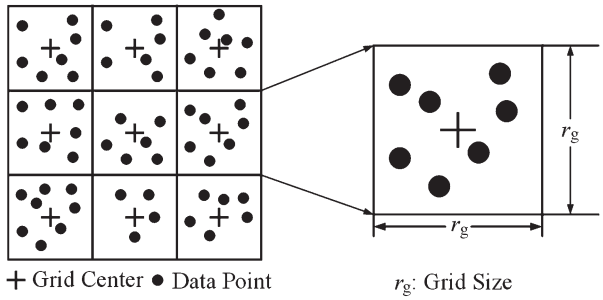

Fig. 1. Gridding model of the road surface point cloud.

intensities of the data points. Then, the manhole and sewer well covers are automatically detected using the proposed marked point process.

II. Rasterization of Road Surface Point Clouds

Instead of processing road surface point clouds in 3-D space, we rasterize the road surface points into a 2-D georeferenced intensity image, in which the gray value of a pixel is interpolated from a group of points based on their intensities. To this end, we first grid and project the road surface point cloud onto the horizontal xy plane (see Fig. 1). Parameter r_g is the grid size or the resolution of the georeferenced intensity image.

We improve the inverse distance weighted (IDW) interpolation method [14] and develop a new strategy to generate the georeferenced intensity image based on the following rules: 1) a point with a larger intensity gets a greater weight; and 2) a point with a distance farther away from the grid center gets a smaller weight. According to these rules, the gray value of the grid cell (i, j), which is denoted by G_{ij}, is calculated by

$$\begin{cases} G_{ij} = \left(\sum_{k=1}^{n_{ij}} W_k^{ij} I_k^{ij}\right) \Big/ \left(\sum_{k=1}^{n_{ij}} W_k^{ij}\right) \\ W_k^{ij} = \alpha W_{k,ij}^D + \beta W_{k,ij}^I, \quad \text{with } \alpha + \beta = 1.0 \end{cases} \tag{1}$$

where n_{ij} is the number of data points within grid cell (i, j); W_k^{ij} and I_k^{ij} are the weight and the intensity of the kth point within grid cell (i, j), respectively. α and β are the weight coefficients; $W_{k,ij}^D$ and $W_{k,ij}^I$ are the weight components calculated considering the planar Euclidean distance from the grid center and the intensity difference within grid cell (i, j), respectively. They are calculated as follows:

$$\begin{cases} W_{k,ij}^D = \frac{1}{r_g^2}\left(\frac{2+r_g^2}{1+D_{k,ij}^2} - 2\right) \\ D_{k,ij} = \sqrt{\left(x_k^{ij} - x_0^{ij}\right)^2 + \left(y_k^{ij} - y_0^{ij}\right)^2} \end{cases} \tag{2}$$

where $D_{k,ij}$ is the planar Euclidean distance between points (x_k^{ij}, y_k^{ij}) and (x_0^{ij}, y_0^{ij}), which are the coordinates of the kth point and the grid center within grid cell (i, j) on the xy plane. In addition,

$$W_{k,ij}^I = W_{k,ij}^{I_1} \cdot W_{k,ij}^{I_2}$$

$$\begin{cases} W_{k,ij}^{I_1} = \frac{1}{\left(g_{\max}^{ij} - g_{\min}^{ij}\right)^2}\left(\frac{1+\left(g_{\max}^{ij} - g_{\min}^{ij}\right)^2}{1+\left(I_k^{ij} - g_{\min}^{ij}\right)^2} - 1\right) \\ W_{k,ij}^{I_2} = \frac{1}{(I_{\max} - I_{\min})^2}\left(\frac{1+(I_{\max} - I_{\min})^2}{1+\left(I_k^{ij} - I_{\min}\right)^2} - 1\right) \end{cases} \tag{3}$$

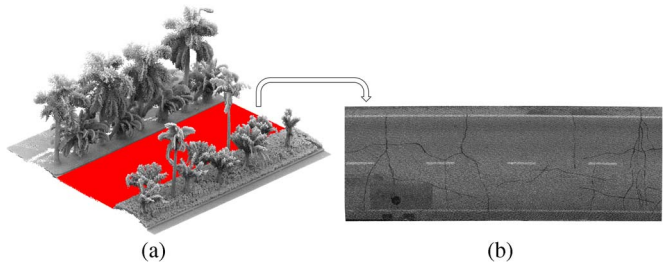

Fig. 2. (a) Mobile LiDAR point cloud with segmented road surface (red). (b) Generated georeferenced intensity image of the road surface point cloud.

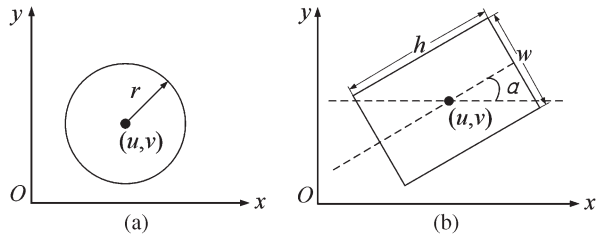

Fig. 3. Marked point models for the (a) manhole and (b) sewer well covers.

where $W_{k,ij}^{I_1}$ and $W_{k,ij}^{I_2}$ are the weight components calculated based on the local and the global intensity information, respectively; $g_{\max}^{ij}$ and $g_{\min}^{ij}$ are the local maximal and minimal intensities within grid cell (i, j); and $I_{\max}$ and $I_{\min}$ are the global maximal and minimal intensities of the point cloud. A generated georeferenced intensity image using the proposed IDW method is shown in Fig. 2.

III. Detection of Manhole and Sewer Well Covers

A. Marked Point Model

As shown in Fig. 3(a), a manhole cover is characterized by a marked point of disk with marks (u, v, r), where (u, v) is the center of the disk, and r is the radius. A sewer well cover is characterized by a marked point of rectangle with marks (u, v, w, h, α), where (u, v) is the center of the rectangle, w and h are the width and height, respectively, and α is the orientation of the rectangle, as shown in Fig. 3(b).

B. Bayesian Model

Consider a georeferenced intensity image $\mathbf{G} = \{g_i = G(x_i, y_i); i = 1, 2, \ldots n, (x_i, y_i) \in D\}$, where (x_i, y_i) is the location of pixel i; g_i, a sample of random variable G at (x_i, y_i), represents the intensity of pixel i; n is the number of pixels in $\mathbf{G}$; and D is the domain of $\mathbf{G}$. In order to distinguish manhole and sewer well covers from the background, D is divided into three regions: $D = \{D_b, D_m, D_s\}$, where D_b, D_m, and D_s correspond to the background, manhole cover, and sewer well cover regions, respectively. $D_m = \{M_j; j = 1, 2, \ldots, k\}$, where M_j is the region of the jth manhole cover, and k denotes the number of manhole covers. $D_s = \{S_j; j = 1, 2, \ldots l\}$, where S_j is the region of the jth sewer well cover, and l denotes the number of sewer well covers. Assume that the intensities in these

three regions are characterized by Gaussian distributions as follows:

$$p(g_i) = \begin{cases} \frac{1}{\sqrt{2\pi}\sigma_b} \exp\left(-\frac{(g_i-\mu_b)^2}{2\sigma_b^2}\right), & (x_i, y_i) \in D_b \\ \frac{1}{\sqrt{2\pi}\tau_j} \exp\left(-\frac{(g_i-\upsilon_j)^2}{2\tau_j^2}\right), & (x_i, y_i) \in M_j \\ \frac{1}{\sqrt{2\pi}\varepsilon_j} \exp\left(-\frac{(g_i-\omega_j)^2}{2\varepsilon_j^2}\right), & (x_i, y_i) \in S_j \end{cases} \quad (4)$$

where μ_b, υ_j, and ω_j are the means; and σ_b, τ_j, and ε_j are the standard deviations of Gaussian distributions for the intensities in the background, the jth manhole cover, and the jth sewer well cover regions, respectively.

Assume that all intensities are independent. Then, the joint distribution for the intensities in each object region is expressed as follows:

$$\begin{cases} p(\mathbf{G}_b) = \Pi_{(x_i,y_i)\in D_b} \frac{1}{\sqrt{2\pi}\sigma_b} \exp\left(-\frac{(g_i-\mu_b)^2}{2\sigma_b^2}\right) \\ \quad \mathbf{G}_b = \{g_i; (x_i, y_i) \in D_b, i \in \{1, 2, \ldots n\}\} \\ p(\mathbf{G}_m) = \Pi_{M_j \in D_m} \Pi_{(x_i,y_i)\in M_j} \frac{1}{\sqrt{2\pi}\tau_j} \exp\left(-\frac{(g_i-\upsilon_j)^2}{2\tau_j^2}\right) \\ \quad \mathbf{G}_m = \{g_i; (x_i, y_i) \in D_m, i \in \{1, 2, \ldots n\}\} \\ p(\mathbf{G}_s) = \Pi_{S_j \in D_s} \Pi_{(x_i,y_i)\in S_j} \frac{1}{\sqrt{2\pi}\varepsilon_j} \exp\left(-\frac{(g_i-\omega_j)^2}{2\varepsilon_j^2}\right) \\ \quad \mathbf{G}_s = \{g_i; (x_i, y_i) \in D_s, i \in \{1, 2, \ldots n\}\}. \end{cases} \quad (5)$$

Denote $\mathbf{B} = \{\mathbf{M}, \mathbf{S}\}$ as the set of manhole and sewer well covers, where $\mathbf{M} = \{\mathbf{C_m}, \mathbf{R}, k\}$ and $\mathbf{S} = \{\mathbf{C_s}, \mathbf{W}, \mathbf{H}, \boldsymbol{\alpha}, l\}$ are the parameter sets of manhole and sewer well covers, respectively. $\mathbf{C_m} = \{(u_j, v_j); j = 1, 2, \ldots k\}$ and $\mathbf{C_s} = \{(u_j, v_j); j = 1, 2, \ldots l\}$ are the centers of manhole and sewer well covers, respectively. $\mathbf{R} = \{r_j;\ j = 1, 2, \ldots k\}$ contains the radii of manhole covers; and $\mathbf{W} = \{w_j;\ j = 1, 2, \ldots l\}$, $\mathbf{H} = \{h_j; j = 1, 2, \ldots l\}$, and $\boldsymbol{\alpha} = (\alpha_j; j = 1, 2, \ldots l)$ contain the widths, heights, and orientations of sewer well covers, respectively. Assume that the centers and orientations uniformly distribute on D and $(-\pi/2, \pi/2]$, respectively; the prior distributions of k and l are assumed to follow Poisson distributions with means λ_m and λ_s [15], and other parameters are assumed to be Gaussian distributions.

By the Bayesian paradigm, the posterior distribution of the parameter set $\mathbf{B}$ conditional on the given georeferenced intensity image $\mathbf{G}$ is expressed as follows:

$$P(\mathbf{B}|\mathbf{G}) \propto P(\mathbf{G}|\mathbf{B})P(\mathbf{B}) \quad (6)$$

where the likelihood $P(\mathbf{G}|\mathbf{B})$ is defined as

$$\begin{aligned} P(\mathbf{G}|\mathbf{B}) &= P(\mathbf{G}|\mathbf{M}, \mathbf{S}) \\ &= P(\mathbf{G}_b)P(\mathbf{G}_m|\mathbf{C}_m, \mathbf{R}, k) \\ &\quad \times P(\mathbf{G}_s|\mathbf{C}_s, \mathbf{W}, \mathbf{H}, \boldsymbol{\alpha}, l) \quad (7) \\ P(\mathbf{B}) &= P(\mathbf{C}_m|k)P(\mathbf{R}|k)P(k)P(\mathbf{C}_s|l) \\ &\quad \times P(\mathbf{W}|l)P(\mathbf{H}|l)P(\boldsymbol{\alpha}|l)P(l). \quad (8) \end{aligned}$$

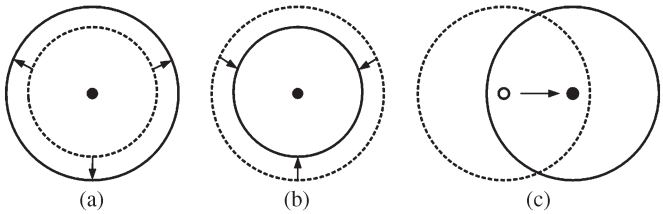

Fig. 4. Transformations for the marked point of disks.

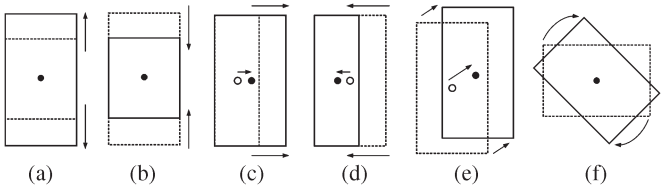

Fig. 5. Transformations for the marked point of rectangles.

C. Simulation and Optimization

The reversible jump Markov chain Monte Carlo (RJMCMC) algorithm [16] is implemented to simulate the posterior distribution in (6). The proposed operations are as follows:

1) *Initialization:* Set the initial number of manhole and sewer well covers, taking $k^0 = 1$ and $l^0 = 1$, for simplicity. Set the initial value of the parameter set $\mathbf{B}^0 = \{\mathbf{M}^0, \mathbf{S}^0\}$, which are drawn from their appropriate distributions. Set the maximum iterations T_m.
2) *Updating marks:* As shown in Figs. 4 and 5, we consider three and six types of transformations for the marked points of disks and rectangles, respectively. For a selected marked point, for example, $\mathbf{M}_j^{(t-1)} = (u_j^{(t-1)}, v_j^{(t-1)}, r_j^{(t-1)})$, $j \in \{1, 2, \ldots k\}$, in the tth iteration, draw a proposal $\mathbf{M}_j^* = (u_j^*, v_j^*, r_j^*)$ from their prior distributions. The center (u_j^*, v_j^*) is uniformly drawn from M_j, and r_j^* is drawn from a Gaussian distribution $N(r_j^{(t-1)}, \delta)$, where δ is the standard deviation. Then, the acceptance probability for the proposal is calculated as follows:

$$r_{\mathbf{B}}\left(\mathbf{B}^*, \mathbf{B}^{(t-1)}\right) = \min\left(1, \frac{P(\mathbf{G}_{M_j^*}|\mathbf{B}^*)P(\mathbf{B}^*)}{P(\mathbf{G}_{M_j}|\mathbf{B}^{(t-1)})P(\mathbf{B}^{(t-1)})}\right) \quad (9)$$

where $\mathbf{B}^* = \{\mathbf{M}^*, \mathbf{S}^{(t-1)}\}$, $\mathbf{M}^* = \{\mathbf{M}_1^{(t-1)}, \ldots \mathbf{M}_{j-1}^{(t-1)}, \mathbf{M}_j^*, \mathbf{M}_{j+1}^{(t-1)}, \ldots \mathbf{M}_k^{(t-1)}, k\}$, M_j^* denotes the region of the jth manhole cover after updating, and $\mathbf{G}_{M_j} = \{g_i; (x_i, y_i) \in M_j, i \in \{1, 2, \ldots n\}\}$ and $\mathbf{G}_{M_j^*} = \{g_i; (x_i, y_i) \in M_j^*, i \in \{1, 2, \ldots n\}\}$ represent the intensity sets corresponding to the jth manhole cover before and after updating. Finally, accept the proposal if and only if the following criterion is met:

$$\mathbf{B}_j^{(t)} = \begin{cases} \mathbf{B}_j^*, & r_{\mathbf{B}} \geq p_f \\ \mathbf{B}_j^{(t-1)}, & r_{\mathbf{B}} < p_f \end{cases} \quad (10)$$

where $p_{\mathbf{f}}$ is a predefined constant false alarm ratio. The updating of the marks of sewer well covers is carried out similarly.

TABLE I
GROUND TRUTH AND DETECTION RESULTS

Ground Truth		Detection Result			Accuracy Evaluation		
Manhole	Sewer Well	Manhole	Sewer Well	False Alarm	Completeness	Correctness	Quality
94	92	89	88	5	95.16%	97.25%	92.67%

3) *Birth or death:* Let the probability of proposing a birth or death operation be b and d, respectively. For a birth operation, draw the marks of the marked point (disk or rectangle) from their prior distributions. For example, for a marked point of disk $\mathbf{M}^*_{k+1}$, draw its center (u^*_{k+1}, v^*_{k+1}) from $D - D_m \cup D_s$ uniformly and draw its radius r^*_{k+1} from a Gaussian distribution. According to the RJMCMC algorithm [16], the acceptance probability for the birth operation is

$$r_b(\mathbf{B}^*, \mathbf{B}) = \min\left(1, \frac{P(\mathbf{G}|\mathbf{B}^*)P(\mathbf{B}^*)j_b(\mathbf{B}^*)}{P(\mathbf{G}|\mathbf{B})P(\mathbf{B})j_d(\mathbf{B})P\left(\mathbf{M}^*_{k+1}\right)}\left|\frac{\partial(\mathbf{B}^*)}{\partial\left(\mathbf{B}, \mathbf{M}^*_{k+1}\right)}\right|\right) \tag{11}$$

where $j_b(\mathbf{B}^*) = b$, $j_d(\mathbf{B}) = (d/k+1)$, $(P(\mathbf{B}^*)/P(\mathbf{B})P(\mathbf{M}^*_{k+1})) = (\lambda_m/k+1)$, and $|\partial(\mathbf{B}^*)/\partial(\mathbf{B}, \mathbf{M}^*_{k+1})| = 1$. For simplicity, let $d = \lambda_m b$, then (11) can be rewritten as

$$r_b(\mathbf{B}^*, \mathbf{B}) = \min\left(1, \frac{P(\mathbf{G}|\mathbf{B}^*)}{P(\mathbf{G}|\mathbf{B})}\right). \tag{12}$$

Then, accept the proposal if and only if $r_b \geq p_f$.

The acceptance probability for the death operation is calculated as follows:

$$r_d(\mathbf{B}^*, \mathbf{B}) = \min\left(1, \frac{P(\mathbf{G}|\mathbf{B})}{P(\mathbf{G}|\mathbf{B}^*)}\right). \tag{13}$$

After the maximum iteration T_m, the maximum *a posteriori* (MAP) criterion is used to obtain the final detection result, i.e.,

$$\hat{\mathbf{B}} = \arg\left\{\max\left(P(\mathbf{B}|\mathbf{G})\right)\right\}. \tag{14}$$

IV. RESULTS AND DISCUSSION

The mobile LiDAR point clouds used in this study were acquired by a RIEGL VMX-450 system integrated with two full-view RIEGL VQ-450 laser scanners in a tropical urban environment, Xiamen, a port city in southeast China. The average density of the point clouds on the road surface is approximately 4000 points/m^2. The accuracy of the acquired point clouds is within 8 mm (1σ standard deviation), and the precision is 5 mm with a maximum effective rate of 1.1 million measurements per second.

A. Detection of Manhole and Sewer Well Covers

To detect road manhole and sewer well covers, a road surface point cloud was selected from the surveyed data with a distance of approximately 3 km along the road. First, we partitioned the road surface point cloud into a group of segments in order to reduce the size of each segment being processed. Next, we rasterized the road surface segments into a group of georeferenced intensity images with a resolution of $r_g = 2.5$ cm and the weight coefficients of $\alpha = 0.5$ and $\beta = 0.5$. Finally, we applied the proposed marked point process based detection algorithm to the generated georeferenced intensity images to detect road manhole and sewer well covers. The ground truth and the detection result are listed in Table I. Compared with the ground truth, the majority of the manhole and sewer well covers were detected with a small number of false alarms. Figs. 6 and 7 show parts of the generated georeferenced intensity images of the road surface point cloud and the corresponding detection results of manhole and sewer well covers. As shown in Fig. 6(b), a dark spot (#1) on the georeferenced intensity image was falsely detected as a manhole cover since the intensity distribution within the dark spot is very similar to that of the manhole covers. However, as shown in Fig. 7(b), two manhole covers (#2 and #3) were undetected since the intensities within these regions are too bright.

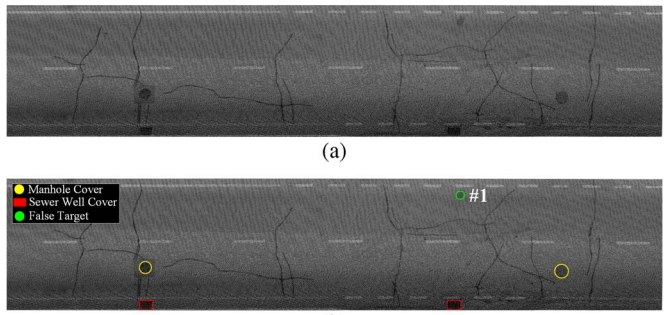

Fig. 6. (a) Georeferenced intensity image. (b) Detected manhole and sewer well covers.

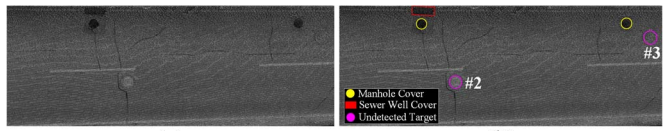

Fig. 7. (a) Georeferenced intensity image. (b) Detected manhole and sewer well covers.

In order to quantitatively evaluate the accuracy of the detection results, we applied three indices presented in [17]: completeness, correctness, and quality. As shown in Table I, our algorithm achieved a completeness of 95.16%, a correctness of 97.25%, and a quality of 92.67%. These results demonstrate that our algorithm is very promising for detecting road manhole and sewer well covers in a tropical urban environment.

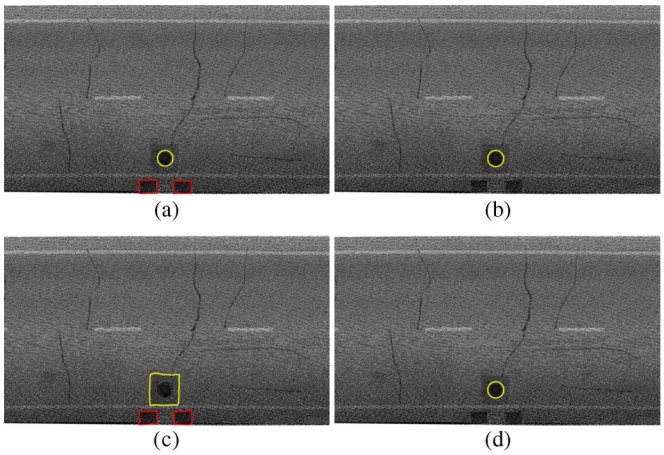

Fig. 8. Detection results of manhole and sewer well covers using (a) our proposed algorithm, (b) the separability and uniformity algorithm, (c) the multiview algorithm, and (d) the Hough transform algorithm.

The proposed algorithm was coded by C++ running on an Intel Xeon workstation with 16 concurrent threads. The total computing time for processing 3-D point clouds covering a 3-km-long road surface is around 9 min.

B. Comparative Study

To further demonstrate the efficiency and correctness of the proposed algorithm, a comparative study was carried out to compare the performance of our proposed algorithm with those of the separability and uniformity [2], multiview [3], and Hough transform algorithms [4]. As shown in Fig. 8, the separability and uniformity algorithm and the Hough transform algorithm both fail to detect the rectangular sewer well covers, whereas the multiview algorithm fails to detect the circular region of the manhole covers. In contrast, our algorithm outperforms the other algorithms in successfully detecting both circular manhole and rectangular sewer well covers.

V. Conclusion

This letter has presented a novel algorithm to automatically detect road manhole and sewer well covers from mobile LiDAR point clouds. A marked point process of disks and rectangles was developed to model the geometric structures and the locations of manhole and sewer well covers. By using marked point processes, the proposed algorithm can process very large volumes of road surface point clouds containing unknown number and sizes of manhole and sewer well covers. The detection results obtained demonstrate that our algorithm can detect manhole and sewer well covers from 3-D point clouds accurately and efficiently with high completeness (95.16%), correctness (97.25%), and quality (92.67%). In addition, a comparative study demonstrates that our algorithm achieved the highest correctness and efficiency over the other three existing algorithms. Instead of processing mobile LiDAR point clouds in 3-D object space on a point-by-point basis, our algorithm rasterized the point clouds into a 2-D georeferenced intensity image so that the detection of manhole and sewer well covers can be implemented in 2-D image space on an object-oriented basis. However, our algorithm is not suitable for detecting manhole and sewer well covers in very high resolution optical images due to their complex texture and intensity distributions.

Acknowledgment

The authors would like to thank the anonymous reviewers for their valuable comments.

References

[1] N. Tanaka and M. Mouri, "A detection method of cracks and structural objects of the road surface image," in *Proc. IAPR Workshop Mach. Vis. Appl.*, Tokyo, Japan, 2000, pp. 387–390.
[2] H. Niigaki, J. Shimamura, and M. Morimoto, "Circular object detection based on separability and uniformity of feature distributions using Bhattacharyya coefficient," in *Proc. 21st Int. Conf. Pattern Recognit.*, Tsukuba, Japan, 2012, pp. 2009–2012.
[3] R. Timofte and L. van Gool, "Multi-view manhole detection, recognition, and 3D localization," in *Proc. IEEE Int. Conf. Comput. Vis. Workshops*, Barcelona, Spain, 2011, pp. 188–195.
[4] Y. Cheng, Z. Xiong, and Y. H. Wang, "Improved classical Hough transform applied to the manhole cover's detection and location," *Opt. Tech.*, vol. 32, no. S1, pp. 504–508, Aug. 2006.
[5] J. Shan and C. Toth, *Topographic Laser Ranging and Scanning: Principles and Processing*. Boca Raton, FL, USA: CRC Press, 2008.
[6] G. Vosselman and H. G. Maas, *Airborne and Terrestrial Laser Scanning*. Boca Raton, FL, USA: CRC Press, 2010.
[7] J. Secord and A. Zakhor, "Tree detection in urban regions using aerial LiDAR and image data," *IEEE Geosci. Remote Sens. Lett.*, vol. 4, no. 2, pp. 196–200, Apr. 2007.
[8] W. Yao and Y. Wei, "Detection of 3-D individual trees in urban areas by combining airborne LiDAR and imagery," *IEEE Geosci. Remote Sens. Lett.*, vol. 10, no. 6, pp. 1355–1359, Nov. 2013.
[9] Y. Yu, J. Li, H. Guan, C. Wang, and M. Cheng, "A marked point process for automated tree detection from mobile laser scanning point cloud data," in *Proc. Comput. Vis. Remote Sens.*, Xiamen, China, 2012, pp. 140–145.
[10] Y. W. Choi, Y. W. Jang, H. J. Lee, and G. S. Cho, "Three-dimensional LiDAR data classifying to extract road point in urban area," *IEEE Geosci. Remote Sens. Lett.*, vol. 5, no. 4, pp. 725–729, Oct. 2008.
[11] B. Yang, W. Xu, and Z. Dong, "Automated extraction of building outlines from airborne laser scanning point clouds," *IEEE Geosci. Remote Sens. Lett.*, vol. 10, no. 6, pp. 1399–1403, Nov. 2013.
[12] B. Yang, Z. Wei, Q. Li, and J. Li, "Semiautomated building facade footprint extraction from mobile LiDAR point clouds," *IEEE Geosci. Remote Sens. Lett.*, vol. 10, no. 4, pp. 766–770, Jul. 2013.
[13] Y. Yu, J. Li, H. Guan, and C. Wang, "A marked point process for automated building detection from LiDAR point-clouds," *Remote Sens. Lett.*, vol. 4, no. 11, pp. 1127–1136, Nov. 2013.
[14] B. Yang, L. Fang, Q. Li, and J. Li, "Automated extraction of road markings from mobile LiDAR point clouds," *Photogramm. Eng. Remote Sens.*, vol. 78, no. 4, pp. 331–338, Apr. 2012.
[15] A. Stoyan, W. S. Kendall, and J. Mecke, *Stochastic Geometry and Its Applications*. Hoboken, NJ, USA: Wiley, 1995.
[16] J. Green, "Reversible jump Markov chain Monte Carlo computation and Bayesian model determination," *Biometrika*, vol. 82, no. 4, pp. 711–732, Dec. 1995.
[17] M. Rutzinger, F. Rottensteiner, and N. Pfeifer, "A comparison of evaluation techniques for building extraction from airborne laser scanning," *IEEE J. Sel. Topics Appl. Earth Observ. Remote Sens.*, vol. 2, no. 1, pp. 11–20, Mar. 2009.